Title

Functional screen identifies kinases driving prostate cancer visceral and bone metastasis

Journal

Proceedings of the National Academy of Sciences of the United States of America, 113(2)

ISSN

0027-8424

Authors

Faltermeier, Claire M

Drake, Justin M

Clark, Peter M

et al.

Publication Date

2016-01-12

DOI

10.1073/pnas.1521674112

Peer reviewed

Functional screen identifies kinases driving prostate cancer visceral and bone metastasis

Claire M. Faltermeier[a], Justin M. Drake[b,1], Peter M. Clark[b], Bryan A. Smith[b], Yang Zong[c], Carmen Volpe[d], Colleen Mathis[b], Colm Morrissey[e], Brandon Castor[f], Jiaoti Huang[f,g,h,i,j], and Owen N. Witte[a,b,c,h,i,j,2]

[a]Molecular Biology Institute, University of California, Los Angeles, CA 90095; [b]Department of Microbiology, Immunology and Molecular Genetics, University of California, Los Angeles, CA 90095; [c]Howard Hughes Medical Institute, University of California, Los Angeles, CA 90095; [d]Division of Laboratory and Animal Medicine, University of California, Los Angeles, CA 90095; [e]Department of Urology, University of Washington, Seattle, WA 98195; [f]Department of Pathology and Laboratory Medicine, University of California, Los Angeles, CA 90095; [g]Department of Urology, University of California, Los Angeles, CA 90095; [h]Jonsson Comprehensive Cancer Center, University of California, Los Angeles, CA 90095; [i]David Geffen School of Medicine, University of California, Los Angeles, CA 90095; and [j]Eli and Edythe Broad Center of Regenerative Medicine and Stem Cell Research, University of California, Los Angeles, CA 90095

Contributed by Owen N. Witte, November 4, 2015 (sent for review September 17, 2015; reviewed by Theresa Guise and John T. Isaacs)

Mutationally activated kinases play an important role in the progression and metastasis of many cancers. Despite numerous oncogenic alterations implicated in metastatic prostate cancer, mutations of kinases are rare. Several lines of evidence suggest that nonmutated kinases and their pathways are involved in prostate cancer progression, but few kinases have been mechanistically linked to metastasis. Using a mass spectrometry-based phosphoproteomics dataset in concert with gene expression analysis, we selected over 100 kinases potentially implicated in human metastatic prostate cancer for functional evaluation. A primary in vivo screen based on overexpression of candidate kinases in murine prostate cells identified 20 wild-type kinases that promote metastasis. We queried these 20 kinases in a secondary in vivo screen using human prostate cells. Strikingly, all three RAF family members, MERTK, and NTRK2 drove the formation of bone and visceral metastasis confirmed by positron-emission tomography combined with computed tomography imaging and histology. Immunohistochemistry of tissue microarrays indicated that these kinases are highly expressed in human metastatic castration-resistant prostate cancer tissues. Our functional studies reveal the strong capability of select wild-type protein kinases to drive critical steps of the metastatic cascade, and implicate these kinases in possible therapeutic intervention.

kinases | metastasis | prostate cancer | bone metastasis

Metastatic prostate cancer is responsible for the deaths of ~30,000 men in the United States each year (1, 2). Ninety percent of patients develop bone metastases, and other major sites of metastases include lymph nodes, liver, adrenal glands, and lung (3). First-line treatments for metastatic disease are androgen deprivation therapies that block androgen synthesis or signaling through the androgen receptor (AR) (2). Inevitably, metastatic prostate cancer becomes resistant to androgen blockade. Second-line treatments such as chemotherapy (docetaxel, cabazitaxel) and radiation only extend survival 2–4 mo (4, 5).

Identifying new therapeutic targets for metastatic prostate cancer has proven difficult. Exome and whole-genome sequencing of human metastatic prostate cancer tissues have found frequent mutations and/or chromosomal aberrations in numerous genes, including *AR*, *TP53*, *PTEN*, *BRCA2*, and *MYC* (6–11). The precise functional contribution of these genes to prostate cancer metastasis remains unknown. Genomic and phosphoproteomic analyses have also revealed that metastatic prostate cancer is molecularly heterogeneous, which has complicated the search for common therapeutic targets (12). Few murine models of prostate cancer develop metastases. Mice having prostate-specific homozygous deletions in *SMAD4* and *PTEN* or expression of mutant *KRAS* develop metastases in visceral organs but rarely in bone (13–15).

Targeting genetically altered constitutively active protein kinases such as BCR-ABL in chronic myelogenous leukemia and $BRAF^{V600E}$ in melanoma has led to dramatic clinical responses (16). Although numerous oncogenic alterations have been identified in prostate cancer, DNA amplifications, translocations, or other mutations resulting in constitutive activity of kinases are rare (6, 9, 17). Genome sequencing of metastatic prostate cancer tissues from >150 patients found translocations involving the kinases BRAF and CRAF in <1% of patients (8, 18). Although uncommon, these genomic aberrations cause enhanced BRAF and CRAF kinase activity and suggest that kinase-driven pathways can be crucial in prostate cancer. Multiple lines of evidence indicate that nonmutated kinases may contribute to prostate cancer progression, castration resistance, and metastasis. SRC kinase synergizes with AR to drive the progression of early-stage prostatic intraepithelial neoplasia to advanced adenocarcinoma (19). SRC, BMX, and TNK2 kinases promote castration resistance by phosphorylating and stabilizing AR (20–22). Moreover, FGFR1, AKT1, and EGFR kinases activate pathways in prostate cancer cells to drive epithelial-to-mesenchymal transition and angiogenesis, both of which are key steps in metastasis (23–25). Despite the strong evidence implicating kinases in advanced prostate cancer, a systematic analysis of the functional role of kinases in prostate cancer metastasis has been lacking.

Metastasis of epithelial-derived cancers encompasses a complex cascade of steps, including (*i*) migration and invasion through

Significance

Therapies are urgently needed to treat metastatic prostate cancer. Mutationally activated and wild-type kinases such as BCR-ABL and BTK are effective therapeutic targets in multiple cancers. Genetically altered kinases are rare in prostate cancer. Wild-type kinases may be implicated in prostate cancer progression, but their therapeutic potential in metastatic prostate cancer remains unknown. Using phosphoproteomics and gene expression datasets, we selected 125 wild-type kinases implicated in human prostate cancer metastasis to screen for metastatic ability in vivo. The RAF family, MERTK, and NTRK2 drove prostate cancer bone and visceral metastasis and were highly expressed in human metastatic prostate cancer tissues. These studies reveal that wild-type kinases can drive metastasis and that the RAF family, MERTK, and NTRK2 may represent important therapeutic targets.

Author contributions: C.M.F. and O.N.W. designed research; C.M.F., J.M.D., P.M.C., B.A.S., Y.Z., C.V., and C. Mathis performed research; C. Morrissey and B.C. contributed new reagents/analytic tools; C.M.F., P.M.C., J.H., and O.N.W. analyzed data; and C.M.F. and O.N.W. wrote the paper.

Reviewers: T.G., Indiana University; and J.T.I., Johns Hopkins Oncology Center.

The authors declare no conflict of interest.

Freely available online through the PNAS open access option.

[1]Present address: Rutgers Cancer Institute of New Jersey and Department of Medicine, Rutgers-Robert Wood Johnson Medical School, New Brunswick, NJ 08901.

[2]To whom correspondence should be addressed. Email: owenwitte@mednet.ucla.edu.

This article contains supporting information online at www.pnas.org/lookup/suppl/doi:10.1073/pnas.1521674112/-/DCSupplemental.

surrounding stroma/basement membrane, (*ii*) intravasation and survival in circulation/lymphatics, (*iii*) extravasation through the vasculature, and (*iv*) survival and growth at a secondary site (26). With the exception of genetically engineered mouse models, no single experimental assay can model all steps of the metastatic cascade. As a result, most screens for genes involved in metastasis have focused on testing one step of the cascade. The migration/invasion step of metastasis is commonly interrogated in vitro by determining the ability of cells to invade through small pores in a membrane (27–29). Genes that function in other steps, or those dependent on the in vivo microenvironment to promote metastasis, are likely to be overlooked in these screens.

Multiple groups have performed in vivo screens for regulators of metastasis by manipulating cell lines in vitro with shRNA libraries or using genome editing techniques, and injecting cells either subcutaneously or into the tail vein of mice (30, 31). These methods are advantageous, because they interrogate multiple steps of the metastatic cascade (survival in circulation, extravasation, and colonization and growth at a secondary site) in a physiologically relevant environment. However, the majority of in vivo screens conducted so far have been based on loss-of-function genetics. These screens are limited to inhibiting the function of proteins expressed by a particular cell line. Using a gain-of-function in vivo screen, we sought to identify kinases that activate pathways leading to prostate cancer metastasis.

Results

Identifying Potential Metastasis-Promoting Kinases Using an Integrated Approach Combining Genomic/Transcriptomic, Phosphoproteomic, and Literature Data. The human kinome encodes over 500 kinases, many of which likely have a limited role in prostate cancer. We reasoned our results would have more relevance if we screened only kinases with evidence of enhanced expression and/or activity in human metastatic prostate cancer. Because no single analysis is both accurate and comprehensive in predicting relevant kinases, three different data sources were investigated. The database cBioPortal contains multiple genomic/transcriptomic datasets from patients with metastatic prostate cancer (6, 9, 32). Five hundred and five kinases were queried for increased RNA expression or genomic amplification in >10% of metastatic patient samples. From this analysis 54 kinases were identified (Table S1). However, high mRNA expression or genomic amplification of a kinase does not always correlate with kinase activity. Identification of phosphorylated kinases or their substrates by phosphoproteomics can better predict kinase activity. Analysis of our previously published phosphoproteomics dataset (33) identified 52 additional kinases with enriched activity in metastatic samples in comparison with benign or localized prostate cancer. Previously published functional studies also provide strong evidence of kinase activity. Searching PubMed using the terms "kinase," "prostate cancer," "metastasis," and "castration resistance" followed by prioritization of articles based on strength of functional data yielded an additional 19 kinases. Our selection method provided 125 kinases for further interrogation of their metastasis-promoting ability (Fig. 1 and Table S1).

Development of an in Vivo Lung Colonization Screen. We devised an in vivo lung colonization screen to test the metastasis-promoting ability of the 125 candidate kinases. A gain-of-function screening design was chosen given our interest in testing whether enhanced expression of a kinase is sufficient to drive metastasis. Additionally, it is unlikely that all 125 kinases are expressed in any single prostate cell line for loss-of-function studies.

Kinases were cloned into a lentiviral expression vector and stably overexpressed in Cap8 cells derived from PTEN null mice (34) (Fig. S1). Cap8 cells have minimal to no metastatic ability in vivo but metastasize when overexpressing a mutationally activated kinase, SRC^{Y529F} (Fig. S2). A luciferase reporter vector was also expressed in Cap8 cells to monitor their metastatic behavior in vivo by bioluminescence imaging (BLI).

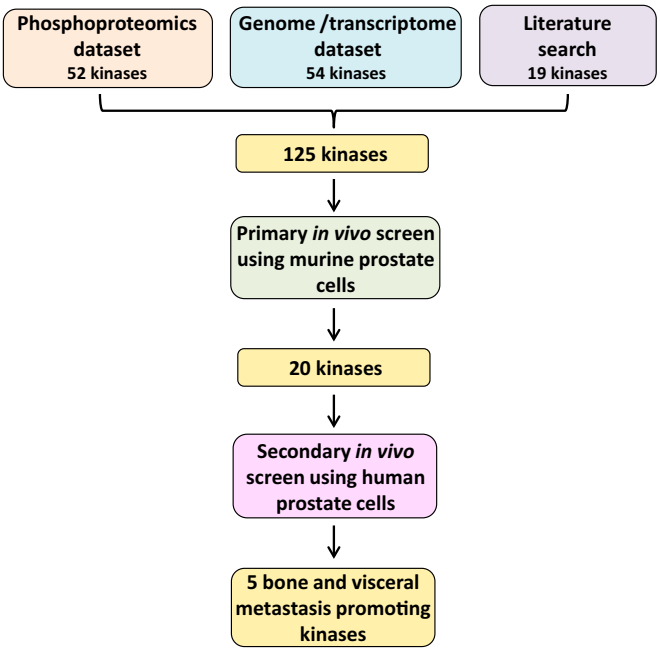

Fig. 1. Schematic summary of the screen for metastasis-promoting kinases. One hundred twenty-five candidate kinases were identified from a combination of genomic/transcriptomic, phosphoproteomic, and literature data. The primary screen entailed expressing all 125 kinases individually in a murine cell line followed by tail vein injection of cells into recipient mice. Twenty kinases strongly promoted lung colonization in vivo. The 20 kinases identified in the primary screen were subjected to a secondary in vivo screen using human prostate cells. Five kinases promoted bone and visceral metastasis in the human cell context.

Testing all 125 kinases as a "pool" in a single mouse would bias our screen toward kinases that are rapid inducers of metastatic colonization. Instead, we decided to test groups of five kinases per mouse to enable identification of kinases with varied metastatic potencies. Groups were selected by choosing five kinases with different molecular weights. Cap8 cells were stably transduced with individual kinases to make 125 different Cap8-kinase cell lines. Equal numbers of five different Cap8-kinase cell lines were pooled and injected into the tail vein of immunocompromised CB17 mice. Because all kinases were cloned with a V5 C-terminal tag (Fig. S1), the metastasis-promoting kinase in each group could be identified by Western blot analysis of the metastatic tissue with a V5 antibody (Fig. 2*A*).

In Vivo Colonization Screen Identifies 20 Kinases That Promote Metastasis in Murine Prostate Cancer Cells. From our screen of 125 kinases, we identified 20 kinases that promoted lung metastasis in vivo (Fig. 2 *B–D*). The most rapid detection of metastasis occurred 2 wk after injection, and was attributed to kinases NTRK2 and MAP3K8. Kinases MAP3K15, MERTK, and all members of the RAF family of kinases (ARAF, BRAF, and CRAF) drove the formation of significant lung metastasis within 3 wks. Kinases promoting metastasis but having a longer latency included FGFR1 (6 wk), SRC (6 wk), and BMX (7 wk) (Figs. 2*D* and 3*A*). Both FGFR1 and SRC have previously described roles in prostate cancer metastasis, which provides support for the validity of our screen (35, 36). Several small lung nodules were recovered at necropsy in 2/5 control mice after 10 wk (Fig. S3*B*). Albeit weak, the inherent metastatic ability of Cap8 cells in our model system implies that the 20 kinases identified are "enhancers of metastasis." It is still unclear whether they are actually "drivers" of de novo metastasis.

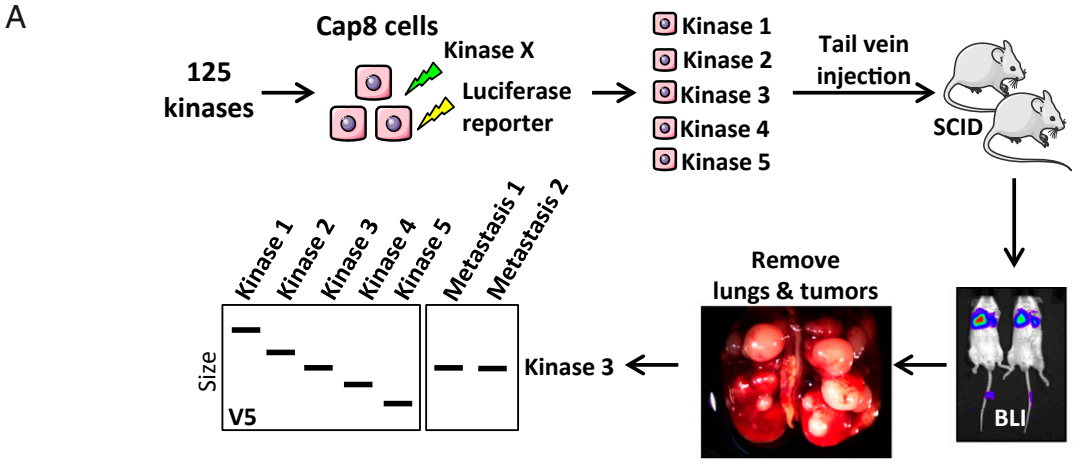

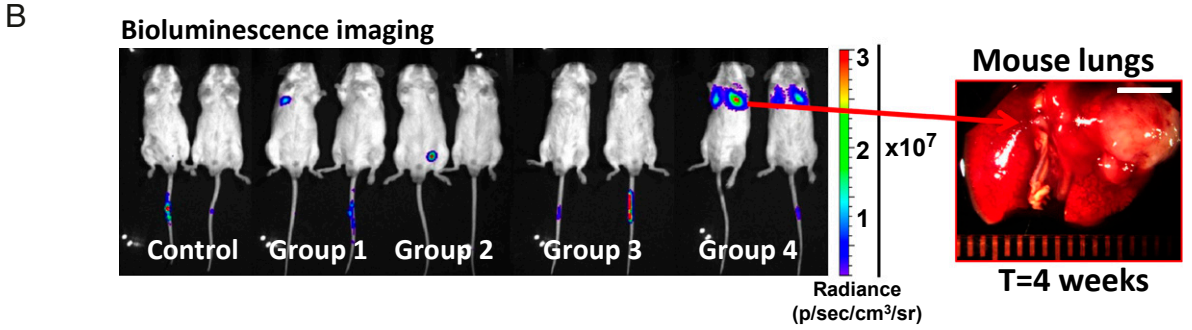

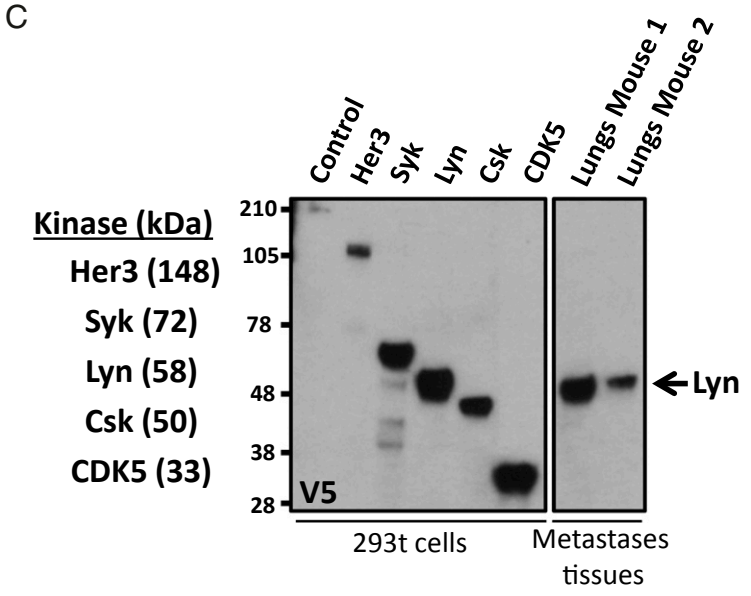

D

Kinase	Latency (weeks)	Kinase	Latency (weeks)
MAP3K8	2	MAP3K2	4
NTRK2	2	NTRK3	4
ARAF	3	PIK3Ca	4
BRAF	3	EGFR	5
CRAF	3	EPHA2	5
MAP3K15	3	HER2	5
MERTK	3	PDGFRa	5
FGFR3	4	FGFR1	6
FLT3	4	SRC	6
LYN	4	BMX	7

Fig. 2. In vivo screen of 125 candidate kinases identifies 20 kinases with metastasis-promoting ability when expressed in murine prostate cells. (*A*) Schematic diagram of the screen testing the metastatic ability of 125 kinases. Kinases were expressed individually in Cap8 cells, pooled into groups of five kinases (each with a different molecular weight), and injected into the tail vein of CB17 SCID mice. Bioluminescence imaging (BLI) was used to detect metastases that were subsequently removed for Western blot analysis. Because all kinases have a C-terminal V5 tag, the Western blot was probed with a V5 antibody to determine which size kinase was enriched in the metastasis tissues. (*B*) Composite BLI image of four different groups of mice. BLI images for each group were taken separately, but at the same time point. Each group was injected with a different set of five kinases. Corresponding bright field image of lungs removed from one of the group 4 mice is shown. sr noted in the units for radiance and refers to steradian. (Scale bar, 5 mm.) (*C*, *Left*) Names and molecular weights of five kinases in a representative group. Western blot analysis of 293t cells overexpressing kinases demonstrates that kinases can be differentiated by size using a V5 antibody. (*C*, *Right*) Western blot of lung tumors removed from mice injected with Cap8 cells overexpressing a group of kinases. By size alignment, the kinase enriched in the metastatic tissue from this particular group was identified as Lyn. (*D*) List of kinases identified in the primary lung colonization screen. Latency columns refer to the interval of time (in weeks) between time of injection and time at which metastatic burden detected by BLI and/or physical symptoms necessitated euthanasia.

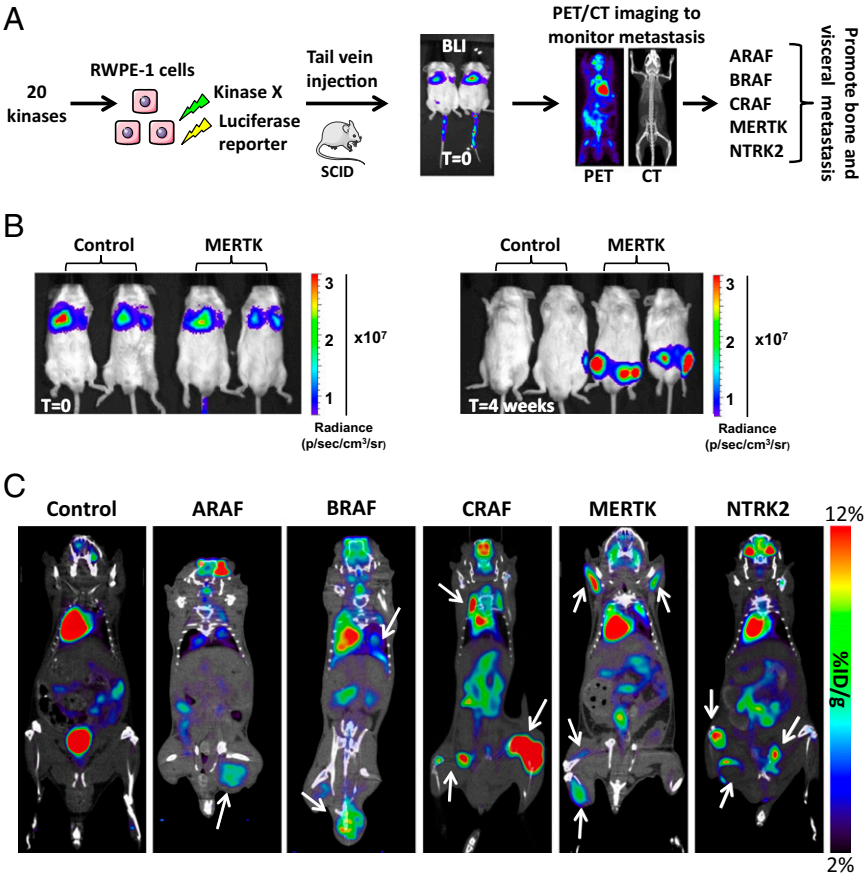

Kinase	Mice	Bone & visceral	Visceral only	No mets	Latency range (M)	Avg. latency (M)	Bone tumor burden
ARAF	8	7	1	0	2-6	4.3	Small
BRAF	4	2	1	1	4-5	4.5	Small
CRAF	6	4	1	1	1-4	2.5	Large
MERTK	6	5	0	1	2-5	3.0	Large
NTRK2	6	4	2	0	2-6	3.3	Large

Fig. 3. Screen of 20 kinases in human prostate cells identifies 5 kinases that drive bone and visceral metastasis. (*A*) Schema of the secondary screen. The 20 kinases identified in the primary screen were expressed in human prostate cells (RWPE-1 cells) and injected into the tail vein of mice. Immediately postinjection, mice were imaged by BLI to verify proper injection. Mice were monitored for metastasis by PET/CT imaging. (*B*) Representative BLI of mice injected with control or MERTK-expressing cells. At time (T) = 0, luciferase signal was detected in the lungs and, by T = 4 wk, luciferase signal was detected in the hind legs. (*C*) PET/CT images of mice injected with control cells or cells expressing the kinases ARAF, BRAF, CRAF, MERTK, and NTRK2. White arrows indicate anatomical sites of high glycolytic activity corresponding to sites of tumor growth. Scale bar on right corresponds to percent injected dose (ID) per gram (g) of tissue. (*D*) Table summarizing the outcomes of tail vein injections of RWPE-1 cells overexpressing ARAF, BRAF, CRAF, MERTK, and NTRK2. Listed are the number of mice tested per kinase, sites of metastatic colonization ("bone & visceral" or "visceral only"), latency (time point at which metastatic burden necessitated euthanasia), and tumor burden. The anatomical sites classified as visceral were lungs and lymph nodes. avg., average; M, month; mets, metastasis.

Screening in Human Prostate Cells Identifies Five Kinases That Drive Bone and Visceral Metastasis in Vivo. To identify which of the 20 candidate kinases drive rather than enhance metastasis in a human cell context, we next assayed their ability to promote metastasis when overexpressed in nonmalignant human prostate cells. The RWPE-1 cell line is derived from normal human prostate epithelium and immortalized with HPV-18 E6/E7 oncogenes (37). RWPE-1 cells do not form colonies in soft agar, nor are they tumorigenic in nude mice (37).

RWPE-1 cells expressing a luciferase reporter gene were separately infected with lentiviruses expressing each of the 20 kinases. Each kinase cell line was individually injected into the tail vein of NOD scid gamma (NSG) mice (Fig. 3*A*). Following tail vein injection, most cells are assumed to get lodged in the small capillaries of the lung rather than travel through the systemic circulation (38). This assumption is consistent with the BLI of mice conducted immediately after injection, showing tumor cells in the lungs but not in other anatomical sites (Fig. 3*B*).

Strikingly, mice injected with cells overexpressing the kinases MERTK, ARAF, BRAF, CRAF, and NTRK2 did not show symptoms of lung metastasis but rather developed hind leg weakness. Mice injected with CRAF-, MERTK-, and NTRK2-expressing RWPE-1 cells were the first to show symptoms 1–2 mo postinjection. A longer latency of up to 6 mo was observed in mice injected with cells expressing ARAF and BRAF. Using BLI, signal was detected in the hind legs (Fig. 3*B*). Although BLI is extremely sensitive, it lacks the precision to accurately predict the location of a metastasis, especially when signal is outside the lungs. Positron-emission tomography combined with computed tomography (PET/CT) is tissue depth-independent and enables precise identification of tumor localization based on cancer cell metabolic activity (39). PET/CT imaging of mice injected with cells expressing MERTK, ARAF, BRAF, CRAF, and NTRK2 showed high [^{18}F]FDG accumulation in the bones, lungs, and lymph nodes (Fig. 3*C*). Control mice were negative for [^{18}F]FDG accumulation in all corresponding anatomical sites (Fig. 3*C*). Further assessment of the CT scans suggested that the bone metastases in mice injected with cells expressing MERTK, ARAF, BRAF, CRAF, and NTRK2 are likely osteolytic.

Histological evaluation of tissues confirmed tumor cell colonization of the lungs, lymph nodes, and bone (femur, tibia, ilium, and vertebra) (Fig. 4 and Figs. S4 and S5). The RAF family members and NTRK2 drove the formation of lung and lymph node metastasis with a similar incidence, whereas MERTK-overexpressing cells did not colonize the lungs (Fig. 3*D*). Although not quantitative,

we observed by histology that metastases driven by CRAF, MERTK, and NTRK2 were extensive, with tumor cells often replacing large areas of bone marrow in the long bones, pelvis, and spine (Figs. 3*D* and 4). In contrast, small metastatic deposits were observed in the femur and spine of mice injected with cells expressing ARAF and BRAF (Fig. 4). To verify that each metastasis expressed the respective kinase and originated from human RWPE-1 cells, bone tissue sections underwent immunohistochemical (IHC) analysis for kinases (MERTK, ARAF, BRAF, CRAF, and NTRK2), HLA, prostate-specific antigen (PSA), and the epithelial cell marker E-cadherin. As shown in Fig. 4, strong IHC staining of each respective kinase, HLA, E-cadherin, and PSA was detected in all bone metastases.

After 8 mo, mice injected with RWPE-1 cells expressing PIK3Cα, MAP3K8, FGFR3, and NTRK3 developed lung, lymph node, and bone micrometastases. None of the mice injected with RWPE-1 cells expressing the other 12 kinases developed metastasis assessed by BLI and histology after 9 mo. Altogether, the functional data described indicate that RAF family members, NTRK2, and MERTK have strong metastasis-promoting ability in both human and mouse prostate cell lines and drive the formation of bone metastasis.

MERTK, NTRK2, and RAF Family Members Are Expressed in Human Prostate Cancer Bone and Visceral Metastasis Tissues. ARAF, BRAF, and CRAF were originally selected for the screen based on predicted activity from our human metastatic prostate cancer phosphoproteomics dataset. Due to the sequence similarity of the RAF kinases (40), some common phosphopeptide substrates could be shared by all three RAF family members. Which RAF family members are relevant to human metastatic prostate cancer remains unclear. MERTK and NTRK2 were added to the screen based on evidence of their role in lung (41), melanoma (42), and glioblastoma metastasis (43), but neither kinase has been previously implicated in prostate cancer metastasis.

To seek evidence of the relevance and therapeutic potential of candidate kinases, we evaluated their expression by immunohistochemistry in metastatic, localized, and benign human prostate cancer tissue samples. The University of Washington's Prostate Cancer Rapid Autopsy Program provided tissue microarrays (TMAs) containing 33 different patients' bone and visceral metastases for staining. We also obtained from the University of California, Los Angeles (UCLA), TMAs containing tissue from 115 patients with benign and medium- to high-grade localized prostate cancer (Gleason 7–9). Because an estimated 10% of patients with

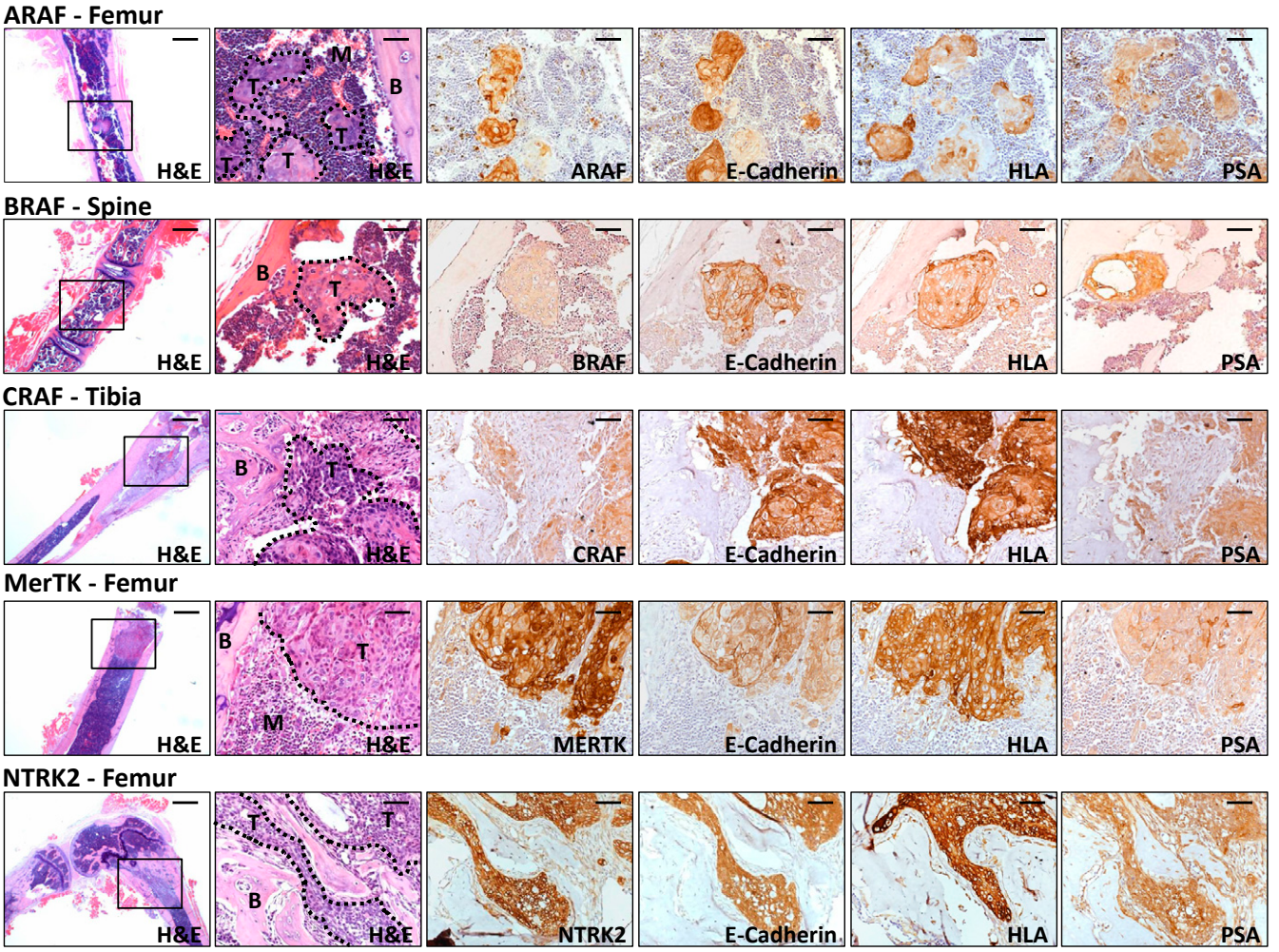

Fig. 4. Histological analysis of bones recovered from mice injected with cells expressing ARAF, BRAF, CRAF, MERTK, and NTRK2 confirms that metastases are of human prostate epithelial cell origin. (*Left* two columns) H&E stains of the affected bones removed from mice injected with RWPE-1 cells expressing the five metastasis-promoting kinases. Images in *Right* five columns are 20× magnification of the area outlined by a black box in the first column. Tumor areas are outlined by black dotted lines and indicated by "T." Bone and bone marrow are marked with "B" and "M," respectively. (*Right* four columns) IHC staining of bone metastasis for overexpressed kinase, E-cadherin, HLA class I, and PSA. [Scale bars, 320 μm (*Left*) and 40 μm (*Right* five columns).]

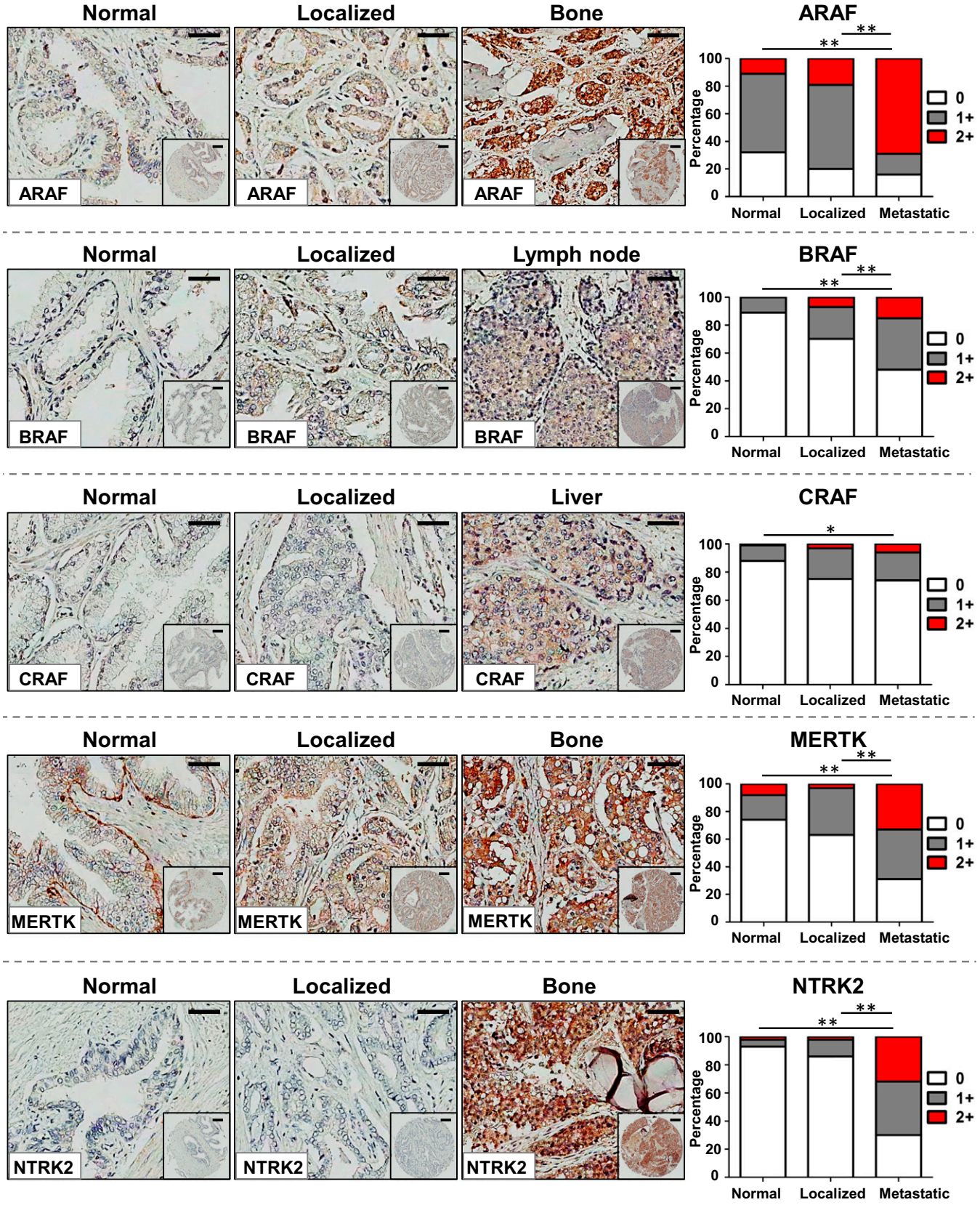

Fig. 5. High levels of the five metastasis-promoting kinases are detected in human prostate cancer metastasis tissues. (*Left*) IHC staining for ARAF, BRAF, CRAF, MERTK, and NTRK2 in representative samples from TMAs containing tissue sections from normal prostate tissue, localized prostate cancer (Gleason 7–9), and metastatic prostate cancer. [Scale bars, 50 μm (large images) and 100 μm (small images).] (*Right*) Quantification of kinase expression in TMAs based on staining intensity. No immunoreactivity was scored as 0, whereas positive immunoreactivity was scored as 1 or 2 based on intensity. The distributions of scores between normal + metastatic tissues and localized + metastatic tissues were subjected to χ^2 statistical analysis. Significance: $^*P \leq 0.05$, $^{**}P \leq 0.01$.

Gleason 7 prostate cancer develop metastasis (44), we hypothesized that the metastasis-promoting kinases would have low expression in the majority of benign and localized prostate cancer tissues in comparison with metastatic prostate cancer tissues.

Consistent with our hypothesis, we found ARAF, BRAF, MERTK, and NTRK2 to be highly expressed in metastatic tissues in comparison with benign or localized prostate cancer tissues (Fig. 5). Remarkably, 69% of metastatic tissues (68/99 samples) had strong ARAF staining (scored as 2+), whereas only 11% of normal (11/102 samples) and 19% of localized prostate cancer tissues (20/105 samples) had ARAF staining of similar intensity. Strong BRAF, MERTK, and NTRK2 staining was detected in 15% (15/100 samples), 33% (32/98 samples), and 32% (31/96 samples) of metastatic tissues, but less than ∼10% of normal and localized prostate cancer tissues were scored 2+ for these three kinases. CRAF-positive staining was higher in metastases (26%, 26/99 samples) in comparison with normal prostate tissue (12%, 11/92 samples). However, no difference in CRAF staining was observed between localized (25%, 24/95 samples) and metastatic prostate cancer. We cannot exclude the possibility that the activation state of CRAF may be different between localized and metastatic prostate cancer samples. Overall, the IHC staining results provide evidence that MERTK, NTRK2, and the RAF family members are expressed and could be functionally relevant in human metastatic prostate cancer. Based on expression, ARAF, BRAF, MERTK, and NTRK2 are more likely to have a functional role in metastasis rather than in early-stage prostate cancer.

Discussion

The strong metastatic ability of RAF family members in our model is consistent with previous reports describing alterations of this pathway in human prostate cancer metastasis. Based on copy number alterations and transcriptome and mutational data, Taylor et al. found that RAS/RAF signaling is dysregulated in 43% of primary tumors and >90% of metastasis (9). Recently, two studies identified BRAF and CRAF fusion proteins with predicted constitutive kinase activity in a small subset (<0.05%) of advanced localized and metastatic prostate cancer tumors (8, 18). We found overexpression of CRAF in the human prostate cell line RWPE-1 to be a more potent driver of bone metastasis (with regard to metastatic burden and time point at which metastases necessitated euthanasia) than ARAF or BRAF. Despite its lower metastatic potency, ARAF expression in human metastatic prostate cancer tissues was much higher than BRAF or CRAF expression. It is possible that ARAF is the dominant RAF family member functioning in human prostate cancer metastasis.

The mechanism by which RAF family members drive metastasis and in particular bone colonization is unknown. Using Madin–Darby canine kidney (MDCK) cells, Lehmann et al. showed that dimerization of CRAF not only induces ERK/MAPK pathway activation but also leads to TGF-β secretion (45). Because the TGF-β signaling pathway is considered one of the key pathways driving prostate cancer bone metastasis (46), CRAF may contribute to metastasis by promoting autocrine TGF-β secretion. Much less is known about the role of ARAF in tumorigenesis, but a recent study showed that ARAF homodimerization or heterodimerization with BRAF enhanced the metastatic ability of lung cancer cells (47).

We also show that MERTK is a potent inducer of prostate cancer metastasis. As a member of the TAM family of tyrosine kinases, MERTK is best-known for its role in promoting phagocytosis of apoptotic cells and dampening the proinflammatory cytokine response (48). MERTK is overexpressed and/or has functional activity in multiple cancers but is rarely genetically amplified or mutated (48). We demonstrate that wild-type MERTK has functional activity in metastasis and is highly expressed in human prostate cancer metastasis tissues. Lending support to our findings are studies demonstrating that MERTK drives migration and invasion in glioblastoma and melanoma cells (42, 43). The downstream pathways activated by MERTK include the RAF/ERK/MAPK, AKT, Stat, and NF-κB pathways (48). Given the metastatic potency of the RAF pathway in our model, MERTK may be dependent on this pathway for its metastatic ability.

NTRK2 and NTRK3, belonging to the neurotrophin family of tyrosine kinases, were also identified in our screen as strong promoters of prostate cancer metastasis. Expression analyses have previously implicated these kinases in prostate cancer. NTRK2 and NTRK3 were undetectable in normal prostate epithelial cells but positive in bone metastasis tissues (49). The precise function of the neurotrophin tyrosine kinases in prostate cancer is unknown. In multiple cancer types, NTRK2 promotes resistance to anoikis (detachment-induced apoptosis), which is a key step in the metastatic cascade (28, 50). Preventing anoikis could be part of the mechanism by which NTRK2 contributes to prostate cancer metastasis.

One of the most interesting features of our metastatic model is the high frequency of metastasis to the lumbar spine, femur, pelvis, and tibia. This bone metastasis pattern is similar to sites of prostate cancer bone metastasis in humans, with the lumbar vertebrae being most common, followed by ribs, pelvis, and long bones (51). Greater than 80% of mice injected with cells overexpressing ARAF (7/8 mice) and MERTK (5/6 mice) developed bone metastasis, whereas BRAF, CRAF, and NTRK2 promoted bone metastasis in at least 50% of mice. In comparison, the few genetically engineered mouse models that develop prostate cancer metastasis have a lower penetrance (12.5–25%) of bone metastases (52–54). Intracardiac or direct bone injection of human prostate cancer cell lines results in a higher frequency of metastasis, but the incidence and location of bone metastasis vary widely between studies (55, 56). The similarities of our model to human prostate cancer and the high frequency of bone metastasis may increase the feasibility of studying the biological mechanisms of prostate cancer bone metastasis. Integrins and chemoattractants such as αVβ3 and SCF1 likely contribute to prostate cancer bone tropism, and our model could provide insights into how certain kinase pathways regulate these bone homing factors (57, 58).

Our results underscore the potential contribution of wild-type kinases to prostate cancer metastasis and provide rationale for therapeutically targeting MERTK, NTRK2, and RAF family members. Currently, there are no selective Food and Drug Administration (FDA)-approved inhibitors of MERTK or NTRK2. The multikinase inhibitor foretinib inhibits MERTK in addition to c-MET and VEGFR (59). Because c-MET inhibition is effective in some patients with metastatic prostate cancer, targeting both MERTK and c-Met with foretinib may be a promising therapeutic approach (60). Pan-NTRK family member inhibitors are excellent therapeutic candidates for prostate cancer, because they would block the bone metastasis-promoting functions of NTRK2 and NTRK3, and NTRK1-mediated bone pain (61). Sorafenib is an FDA-approved small-molecule inhibitor targeting RAF family members and other kinases such as VEGFR-2, VEGFR-3, and PDGF-β (62). Clinical studies involving a small number of patients have suggested that sorafenib may have therapeutic benefit in patients with castration-resistant prostate cancer (63, 64). Due to reports of paradoxical RAF inhibitor-mediated RAF activation, inhibiting the direct downstream targets of RAF, MEK1/MEK2, may be a better approach (65). Trametinib, an inhibitor of MEK1/MEK2, is currently in phase II clinical trials for patients with advanced prostate cancer (66). Future studies should focus on inhibition of MERTK, NTRK2, and RAF pathways in metastatic models to provide additional rationale for targeting these kinases in patients with metastatic prostate cancer.

Methods

Cell Culture and Reagents. Cap8 cells were obtained from the laboratory of Hong Wu, University of California, Los Angeles (UCLA), and propagated in DMEM supplemented with 10% (vol/vol) FBS (Gibco), 25 μg/mL bovine

pituitary extract (Lonza), 5 μg/mL human insulin (Gibco), 6 ng/mL recombinant human epidermal growth factor (PeproTech), glutamine (1 mM), penicillin (100 U/mL), and streptomycin (100 μg/mL) (34). RWPE-1 cells were purchased from ATCC and cultured in keratinocyte serum-free medium (K-SFM) (Gibco) supplemented with 0.05 mg/mL bovine pituitary extract (Gibco), 5 ng/mL EGF (Gibco), penicillin (100 U/mL), and streptomycin (100 μg/mL). 293t cells used for lentiviral production were cultured in DMEM supplemented with 10% (vol/vol) FBS, glutamine (1 mM), penicillin (100 U/mL), and streptomycin (100 μg/mL).

Cloning of Kinases. We obtained the Center for Cancer Systems Biology–Dana-Farber Cancer Institute–Broad Human Kinase ORF collection consisting of 559 kinases in pDONR-223 Gateway entry vectors. The plasmid kit (Addgene Kit 1000000014) was a gift from William Hahn and David Root, Broad Institute of Harvard and Massachusetts Institute of Technology, Boston. Using the pcDNA 6.2/V5-DEST (Invitrogen), we cloned the attR1-ccdB-CmR-attR2-V5-SV40-blasticidin cassette into the previously described third-generation lentiviral FUCGW vector (67). The FU-R1-R2-V5-SV40-Blasti-CGW vector (Fig. S1) is optimized for our screen based on the V5 tag enabling kinase detection with V5 antibody and selection of kinase-expressing cells using blasticidin. Kinases in pDONR-223 vectors were cloned into FU-R1-R2-V5-SV40-Blasti-CGW using LR Clonase II (Invitrogen) and sequenced to verify the wild-type sequence. Wild-type BRAF and RPS6KA4 were not included in the ORF kinase collection. We acquired these ORFs from the Harvard PlasmID Repository and subcloned them into the FUCGW vector.

Virus Production. Third-generation lentiviruses were prepared by calcium phosphate precipitation transfection of 293t cells with plasmids expressing kinases (FU-kinase-V5-SV40-Blasti-CGW) or luciferase (FU-ILYW). The lentiviruses were prepared as described (67).

Western Blot. Whole-cell lysates were prepared in RIPA lysis buffer (150 nM NaCl, 1% Nonidet P-40, 0.5% sodium deoxycholate, 0.1% SDS, 50 mM Tris, pH 8.0) with phosphatase inhibitor (cocktails 2 and 3; Sigma) and protease inhibitor cocktail (Roche). Equal amounts of protein were separated by 4–20% (mass/vol) Tris-Hepes SDS/PAGE (Thermo Fisher), followed by immunoblotting analysis with the indicated antibodies.

Kinase protein expression was detected using a V5 antibody (Invitrogen R960-25; 1:2,500). Because AXL and BRAF lacked a V5 tag, we verified their expression using an AXL antibody (Cell Signaling 4977; 1:1,000) and a BRAF antibody (Cell Signaling 55C6; 1:1,000).

Animal Studies. All animal experiments were performed according to the protocol approved by the Division of Laboratory Medicine at the University of California, Los Angeles. NOD.CB17-Prkdc^{scid}/J mice (for the primary screen) and NOD-scid gamma (for the secondary screen) were purchased from Jackson Laboratories. For all experiments, male mice between 6 and 8 wk of age were used.

Primary in Vivo Kinase Screen.

Infection of cells and tail vein injections. Cap8 cells were infected with lentivirus expressing luciferase and YFP (FU-ILYW) at a multiplicity of infection (MOI) of 10. Three days later, cells were sorted based on YFP expression using a BD FACSAria. Cap8-ILYW cells were expanded and frozen in aliquots so that all experiments would start at the same cell passage number. Upon starting an experiment, Cap8-ILYW cells were thawed and propagated for 5 d followed by infection with kinases individually at an MOI of 8 in media containing polybrene (8 μg/mL). Twenty-four hours after infection, media was removed and replaced with media containing 13 μg/mL blasticidin (InvivoGen). Cells underwent blasticidin selection for 5 d, followed by propagation for 48 h in complete media (without blasticidin). Instead of screening 125 kinases individually in vivo, we tested groups of 5 kinases in each mouse. Five kinases with different molecular weights were selected for each group. Each group was prepared by counting 2×10^5 cells of each of the five kinase cell lines and pooling the kinase cell lines together in 200 μL HBSS (Life Technologies). Using a 27-G needle, 200 μL (1×10^6 total cells) was injected into the lateral tail vein of CB17 mice in duplicate. D-luciferin substrate was injected i.p. into mice, followed by BLI to verify proper tail vein injection of kinase-expressing Cap8-ILYW cells (indicated by luciferase signal in the lungs). Mice were monitored for physical symptoms of metastasis (labored breathing, cachexia, difficulty moving) and by biweekly BLI. Upon detection of metastasis, mice were euthanized and lung tumors were dissected and stored at −80 °C.

Identification of metastasis-promoting kinase. Lung tumors were thawed, homogenized, and sonicated in RIPA lysis buffer. After a high-speed spin, protein concentration of the supernatant was measured in preparation for Western blotting. Because all kinases had a V5 C-terminal tag, the Western blot was probed with a V5 antibody to determine which size kinase was enriched in the metastasis tissues. To aid in identifying the enriched kinase, we included on our Western blot lysate from 293t cells expressing the five kinase cell lines individually. This Western blot was used as a reference of the individual kinase sizes. For the majority of the metastasis tissues analyzed by Western blot, only one out of the five kinases was enriched. If >1 kinase was identified in the metastasis tissues by Western blot, tail vein injections using cell lines expressing each of the kinases were repeated.

Secondary in Vivo Kinase Screen.

Infection of cells and tail vein injections. The same infection method described for the primary screen was used to transduce RWPE-1 cells with a lentivirus expressing luciferase followed by lentiviruses expressing the 20 kinases (identified in the primary screen). RWPE-1 cells expressing kinases were selected with 15 μg/mL blasticidin for 5 d and prepared for tail vein injection following the method described for the primary screen. However, instead of screening 5 kinases at a time, the 20 kinases were tested individually. Kinase-expressing RWPE-1 cells (1×10^6) were injected into the lateral tail vein of NSG mice in duplicate. D-luciferin substrate was injected i.p. into mice, followed by BLI to verify proper tail vein injection. Mice were monitored for physical symptoms of metastasis and by biweekly BLI. Upon symptom detection or positive BLI signal, mice underwent PET/CT imaging and were euthanized the following day. Macroscopic tumors and bones were removed and prepared for histology. Three biological replicates were performed for each of the five kinases (ARAF, BRAF, CRAF, NTRK2, and MERTK).

Imaging.

Bioluminescence imaging. BLI was conducted using an IVIS Lumina II (PerkinElmer). D-luciferin (150 mg/kg) was injected intraperitoneally. After 15 min, anesthetized mice [using 2.5% (vol/vol) isoflurane] were imaged. BLI analysis was performed using Living Image software, version 4.0 (PerkinElmer).

PET imaging. Mice were placed on a heated platform and anesthetized with 1.5% (vol/vol) isoflurane for the entirety of the experiment. Approximately 740 kBq of ^{18}F-labeled 2-fluoro-2-deoxyglucose ([^{18}F]FDG; obtained from the UCLA Department of Nuclear Medicine) was injected into the tail vein. After 1 h, the mice were imaged for 10 min on a Genisys 4 imager (Sofie Biosciences) followed by a high-resolution computed tomography scan on a CrumpCAT imager (UCLA).* PET and CT images were manually coregistered. Images were analyzed using AMIDE medical imaging software (68).

Immunohistochemistry. Metastatic tissues were removed from the mice and fixed in 10% (vol/vol) formalin overnight and paraffin-embedded. Bones were decalcified before paraffin embedding. Four-micrometer-thick sections were stained with hematoxylin and eosin for representative histology. For IHC analysis of TMAs, sections were heated at 65 °C for 1 h followed by deparaffinization in xylene and rehydration in 100%, 95%, and 70% (vol/vol) ethanol. Antigen retrieval was performed by heating samples at 95° for 20 min in 0.01 M citrate buffer (pH 6.0). Endogenous peroxidase activity was blocked with 3% (vol/vol) H_2O_2 for 10 min, followed by blocking for nonspecific binding with 2.5% (vol/vol) horse serum (Vector Laboratories) for 1 h. Primary antibodies (see below) were diluted in 2.5% (vol/vol) horse serum and incubated on slides overnight at 4 °C. Following three washes with 1× PBS, slides were incubated with anti-mouse HRP or anti-rabbit HRP secondary antibodies (Dako) for 1 h at 25 °C. Slides were developed using the liquid DAB+ Substrate Chromogen System (Dako), counterstained with hematoxylin, dehydrated, and mounted.

MERTK protocol. IHC staining for MERTK was conducted as described (69). Briefly, we followed the same primary antibody protocol as described above, but to increase the sensitivity of MERTK staining we used a biotinylated secondary antibody (goat anti-rabbit IgG; Boster Biotechnology), followed by peroxidase-conjugated streptavidin (SABC; SA1022; Boster Biotechnology). The slide development protocol was followed as described above.

Antibodies. The following primary antibodies and dilutions were used: E-cadherin (BD clone 36; 1:250), PSA (Dako; 1:2,000), HLA class I ABC (Abcam 70328; 1:350), ARAF (Abcam 200653; 1:700), BRAF (Cell Signaling 55C6; 1:100), CRAF (Cell Signaling 9422; 1:100), MERTK (Abcam 52968; 1:300), and NTRK2 (Cell Signaling 4607; 1:250). Dilutions were optimized on sections using metastatic tissues recovered from mice injected with RWPE-1 cells overexpressing each kinase. To ensure specificity and lack of cross-reactivity of RAF family member antibodies, we stained ARAF-overexpressing tissue with BRAF and CRAF antibodies, BRAF-overexpressing tissue with CRAF and ARAF antibodies, and CRAF-overexpressing tissue with ARAF and BRAF antibodies.

*Taschereau R, Vu NT, Chatziioannou AF, 2014 Institute of Electrical and Electronics Engineers Nuclear Science Symposium & Medical Imaging Conference, November 8–15 2014, Seattle, WA.

Clinical Prostate Tissue Microarrays.

Human metastatic prostate cancer tissue microarrays.

Tissue acquisition. Samples were obtained from patients who died of metastatic castration resistant prostate cancer (CRPC) and who signed written informed consent for a rapid autopsy performed within 6 h of death, under the aegis of the Prostate Cancer Donor Program at the University of Washington (70). The Institutional Review Board of the University of Washington approved this study. Visceral metastases were identified at the gross level, bone biopsies were obtained according to a template from 20 different sites, and metastases were identified at a histological level.

Tissue microarray construction. One hundred and three CRPC metastases (including 45 visceral metastases and 58 bone metastases) from 33 autopsy patients (up to four sites per patient) were fixed in buffered formalin [bone metastases were decalcified in 10% (vol/vol) formic acid] and embedded in paraffin. A TMA was made using duplicate 1-mm-diameter cores from these tissues.

Human benign prostate and localized prostate cancer tissue microarrays. Construction of TMAs was approved by UCLA's Institutional Review Board. Samples were obtained from prostatectomy specimens performed at UCLA between 2001 and 2010. A total of 115 cases of high-grade prostate adenocarcinoma (combined Gleason score 7–9) were selected. Three cores of tumor and three cores of corresponding benign prostate were obtained from each case and transferred to two recipient TMA blocks.

Scoring of TMAs. TMAs were scored 0, 1, and 2 based on intensity of staining, with 0 indicating no staining, 1 indicating weakly positive staining, and 2 indicating strongly positive staining. Two separate observers scored normal prostate, localized prostate cancer, and metastatic prostate cancer TMAs. TMAs and corresponding scores were reviewed by a board-certified pathologist. Because MERTK is expressed in normal human prostate basal cells and in macrophages, scores for MERTK were based on expression only in luminal cells. Representative images of TMAs were taken using a Zeiss Axio Imager A1 microscope. To optimize TMA images for print (Fig. 5), PowerPoint was used to equally adjust all images using the following parameters: sharpen (+25%), brightness (–33%), and contrast (+66%).

ACKNOWLEDGMENTS. We thank members of the O.N.W. laboratory for helpful comments and discussion. We are grateful to the patients and their families who were willing to participate in the University of Washington's Prostate Cancer Donor Program and the investigators Drs. Robert Vessella, Celestia Higano, Bruce Montgomery, Evan Yu, Peter Nelson, Paul Lange, Martine Roudier, and Lawrence True and the Rapid Autopsy team for their contributions to the University of Washington Medical Center Prostate Cancer Donor Rapid Autopsy Program. This research was supported by funding from the Pacific Northwest Prostate Cancer Specialized Program of Research Excellence (SPORE) (P50CA97186) and a P01 NIH grant (P01CA085859). We thank Dr. Daniel Margolis for radiological evaluation of PET/CT scans; UCLA Molecular Imaging Center and staff; H. Wu laboratory for cell lines; UCLA Translational Pathology Core Laboratory for assistance with tissue processing and H&E staining; and Donghui Cheng for help with FACS sorting. C.M.F. was supported by a California Institute of Regenerative Medicine Training Grant (TG2-01169) and USHHS Ruth L. Kirschstein Institutional National Research Service Award (T32 CA009056); J.M.D. was supported by the Department of Defense Prostate Cancer Research Program (W81XWH-14-1-0148); P.M.C. was supported by a California Institute of Regenerative Medicine Training Grant (TG2-01169), UCLA Scholars in Oncologic Molecular Imaging Program National Cancer Institute Grant (R25T CA098010), and UCLA in Vivo Cellular and Molecular Imaging Center Career Development Award (P50 CA086306); and B.A.S. was supported by a UCLA Tumor Immunology Training Grant (T32 CA00912). J.H. is supported by NIH Grants 5R01CA172603-02 [principal investigator (PI): J.H.], 2P30CA016042-39 (PI: Judith Gasson), 1R01CA181242-01A1 (PI: Chun Chao), and 1R01CA195505 (PI: Leonard Marks); Department of Defense Prostate Cancer Research Program W81XWH-12-1-0206 (PI: Lily Wu); UCLA SPORE in prostate cancer (PI: Robert Reiter); Prostate Cancer Foundation Honorable A. David Mazzone Special Challenge Award (PI: Robert Reiter); and UCLA Jonsson Comprehensive Cancer Center Impact Grant (PI: Sanaz Memarzadeh). O.N.W. is an Investigator of the Howard Hughes Medical Institute and is supported by a Prostate Cancer Foundation Challenge Award. J.H. and O.N.W. are supported by a Stand Up To Cancer–Prostate Cancer Foundation Prostate Dream Team Translational Research Grant (SU2C-AACR-DT0812). This research grant is made possible by the generous support of the Movember Foundation. Stand Up To Cancer is a program of the Entertainment Industry Foundation administered by the American Association for Cancer Research.

1. van Dodewaard-de Jong JM, et al. (2015) New treatment options for patients with metastatic prostate cancer: What is the optimal sequence? *Clin Genitourin Cancer* 13(4):271–279.
2. Nelson WG, De Marzo AM, Isaacs WB (2003) Prostate cancer. *N Engl J Med* 349(4): 366–381.
3. Bubendorf L, et al. (2000) Metastatic patterns of prostate cancer: An autopsy study of 1,589 patients. *Hum Pathol* 31(5):578–583.
4. de Bono JS, et al.; TROPIC Investigators (2010) Prednisone plus cabazitaxel or mitoxantrone for metastatic castration-resistant prostate cancer progressing after docetaxel treatment: A randomised open-label trial. *Lancet* 376(9747):1147–1154.
5. Parker C, et al.; ALSYMPCA Investigators (2013) Alpha emitter radium-223 and survival in metastatic prostate cancer. *N Engl J Med* 369(3):213–223.
6. Grasso CS, et al. (2012) The mutational landscape of lethal castration-resistant prostate cancer. *Nature* 487(7406):239–243.
7. Gundem G, et al.; ICGC Prostate UK Group (2015) The evolutionary history of lethal metastatic prostate cancer. *Nature* 520(7547):353–357.
8. Robinson D, et al. (2015) Integrative clinical genomics of advanced prostate cancer. *Cell* 161(5):1215–1228.
9. Taylor BS, et al. (2010) Integrative genomic profiling of human prostate cancer. *Cancer Cell* 18(1):11–22.
10. Hong MK, et al. (2015) Tracking the origins and drivers of subclonal metastatic expansion in prostate cancer. *Nat Commun* 6:6605.
11. Kumar A, et al. (2011) Exome sequencing identifies a spectrum of mutation frequencies in advanced and lethal prostate cancers. *Proc Natl Acad Sci USA* 108(41): 17087–17092.
12. Drake JM, et al. (2013) Metastatic castration-resistant prostate cancer reveals intrapatient similarity and interpatient heterogeneity of therapeutic kinase targets. *Proc Natl Acad Sci USA* 110(49):E4762–E4769.
13. Aytes A, et al. (2013) ETV4 promotes metastasis in response to activation of PI3-kinase and Ras signaling in a mouse model of advanced prostate cancer. *Proc Natl Acad Sci USA* 110(37):E3506–E3515.
14. Mulholland DJ, et al. (2012) Pten loss and RAS/MAPK activation cooperate to promote EMT and metastasis initiated from prostate cancer stem/progenitor cells. *Cancer Res* 72(7):1878–1889.
15. Ding Z, et al. (2011) SMAD4-dependent barrier constrains prostate cancer growth and metastatic progression. *Nature* 470(7333):269–273.
16. Zhang J, Yang PL, Gray NS (2009) Targeting cancer with small molecule kinase inhibitors. *Nat Rev Cancer* 9(1):28–39.
17. Drake JM, Lee JK, Witte ON (2014) Clinical targeting of mutated and wild-type protein tyrosine kinases in cancer. *Mol Cell Biol* 34(10):1722–1732.
18. Palanisamy N, et al. (2010) Rearrangements of the RAF kinase pathway in prostate cancer, gastric cancer and melanoma. *Nat Med* 16(7):793–798.
19. Cai H, Babic I, Wei X, Huang J, Witte ON (2011) Invasive prostate carcinoma driven by c-Src and androgen receptor synergy. *Cancer Res* 71(3):862–872.
20. Dai B, et al. (2010) Compensatory upregulation of tyrosine kinase Etk/BMX in response to androgen deprivation promotes castration-resistant growth of prostate cancer cells. *Cancer Res* 70(13):5587–5596.
21. Guo Z, et al. (2006) Regulation of androgen receptor activity by tyrosine phosphorylation. *Cancer Cell* 10(4):309–319.
22. Mahajan NP, et al. (2007) Activated Cdc42-associated kinase Ack1 promotes prostate cancer progression via androgen receptor tyrosine phosphorylation. *Proc Natl Acad Sci USA* 104(20):8438–8443.
23. Acevedo VD, et al. (2007) Inducible FGFR-1 activation leads to irreversible prostate adenocarcinoma and an epithelial-to-mesenchymal transition. *Cancer Cell* 12(6): 559–571.
24. Gan Y, et al. (2010) Differential roles of ERK and Akt pathways in regulation of EGFR-mediated signaling and motility in prostate cancer cells. *Oncogene* 29(35):4947–4958.
25. Conley-LaComb MK, et al. (2013) PTEN loss mediated Akt activation promotes prostate tumor growth and metastasis via CXCL12/CXCR4 signaling. *Mol Cancer* 12(1):85.
26. Nguyen DX, Bos PD, Massagué J (2009) Metastasis: From dissemination to organ-specific colonization. *Nat Rev Cancer* 9(4):274–284.
27. van Roosmalen W, et al. (2015) Tumor cell migration screen identifies SRPK1 as breast cancer metastasis determinant. *J Clin Invest* 125(4):1648–1664.
28. Douma S, et al. (2004) Suppression of anoikis and induction of metastasis by the neurotrophic receptor TrkB. *Nature* 430(7003):1034–1039.
29. Scott KL, et al. (2011) Proinvasion metastasis drivers in early-stage melanoma are oncogenes. *Cancer Cell* 20(1):92–103.
30. Chen S, et al. (2015) Genome-wide CRISPR screen in a mouse model of tumor growth and metastasis. *Cell* 160(6):1246–1260.
31. Duquet A, et al. (2014) A novel genome-wide in vivo screen for metastatic suppressors in human colon cancer identifies the positive WNT-TCF pathway modulators TMED3 and SOX12. *EMBO Mol Med* 6(7):882–901.
32. Cerami E, et al. (2012) The cBio Cancer Genomics Portal: An open platform for exploring multidimensional cancer genomics data. *Cancer Discov* 2(5):401–404.
33. Drake JM, et al. (2012) Oncogene-specific activation of tyrosine kinase networks during prostate cancer progression. *Proc Natl Acad Sci USA* 109(5):1643–1648.
34. Jiao J, et al. (2007) Murine cell lines derived from Pten null prostate cancer show the critical role of PTEN in hormone refractory prostate cancer development. *Cancer Res* 67(13):6083–6091.
35. Park SI, et al. (2008) Targeting SRC family kinases inhibits growth and lymph node metastases of prostate cancer in an orthotopic nude mouse model. *Cancer Res* 68(9): 3323–3333.
36. Yang F, et al. (2013) FGFR1 is essential for prostate cancer progression and metastasis. *Cancer Res* 73(12):3716–3724.
37. Bello D, Webber MM, Kleinman HK, Wartinger DD, Rhim JS (1997) Androgen responsive adult human prostatic epithelial cell lines immortalized by human papillomavirus 18. *Carcinogenesis* 18(6):1215–1223.

38. Fidler IJ (2003) The pathogenesis of cancer metastasis: The 'seed and soil' hypothesis revisited. *Nat Rev Cancer* 3(6):453–458.
39. Gambhir SS (2002) Molecular imaging of cancer with positron emission tomography. *Nat Rev Cancer* 2(9):683–693.
40. Leicht DT, et al. (2007) Raf kinases: Function, regulation and role in human cancer. *Biochim Biophys Acta* 1773(8):1196–1212.
41. Sinkevicius KW, et al. (2014) Neurotrophin receptor TrkB promotes lung adenocarcinoma metastasis. *Proc Natl Acad Sci USA* 111(28):10299–10304.
42. Schlegel J, et al. (2013) MERTK receptor tyrosine kinase is a therapeutic target in melanoma. *J Clin Invest* 123(5):2257–2267.
43. Wang Y, et al. (2013) Mer receptor tyrosine kinase promotes invasion and survival in glioblastoma multiforme. *Oncogene* 32(7):872–882.
44. Partin AW, et al. (1997) Combination of prostate-specific antigen, clinical stage, and Gleason score to predict pathological stage of localized prostate cancer. A multi-institutional update. *JAMA* 277(18):1445–1451.
45. Lehmann K, et al. (2000) Raf induces TGFbeta production while blocking its apoptotic but not invasive responses: A mechanism leading to increased malignancy in epithelial cells. *Genes Dev* 14(20):2610–2622.
46. Fournier PG, et al. (2015) The TGF-β signaling regulator PMEPA1 suppresses prostate cancer metastases to bone. *Cancer Cell* 27(6):809–821.
47. Mooz J, et al. (2014) Dimerization of the kinase ARAF promotes MAPK pathway activation and cell migration. *Sci Signal* 7(337):ra73.
48. Graham DK, DeRyckere D, Davies KD, Earp HS (2014) The TAM family: Phosphatidylserine sensing receptor tyrosine kinases gone awry in cancer. *Nat Rev Cancer* 14(12):769–785.
49. Dionne CA, et al. (1998) Cell cycle-independent death of prostate adenocarcinoma is induced by the trk tyrosine kinase inhibitor CEP-751 (KT6587). *Clin Cancer Res* 4(8): 1887–1898.
50. Geiger TR, Peeper DS (2007) Critical role for TrkB kinase function in anoikis suppression, tumorigenesis, and metastasis. *Cancer Res* 67(13):6221–6229.
51. Knudson G, et al. (1991) Bone scan as a stratification variable in advanced prostate cancer. *Cancer* 68(2):316–320.
52. Klezovitch O, et al. (2004) Hepsin promotes prostate cancer progression and metastasis. *Cancer Cell* 6(2):185–195.
53. Ding Z, et al. (2012) Telomerase reactivation following telomere dysfunction yields murine prostate tumors with bone metastases. *Cell* 148(5):896–907.
54. Grabowska MM, et al. (2014) Mouse models of prostate cancer: Picking the best model for the question. *Cancer Metastasis Rev* 33(2-3):377–397.
55. Jin JK, Dayyani F, Gallick GE (2011) Steps in prostate cancer progression that lead to bone metastasis. *Int J Cancer* 128(11):2545–2561.
56. Wu TT, et al. (1998) Establishing human prostate cancer cell xenografts in bone: Induction of osteoblastic reaction by prostate-specific antigen-producing tumors in athymic and SCID/bg mice using LNCaP and lineage-derived metastatic sublines. *Int J Cancer* 77(6):887–894.
57. McCabe NP, De S, Vasanji A, Brainard J, Byzova TV (2007) Prostate cancer specific integrin alphavbeta3 modulates bone metastatic growth and tissue remodeling. *Oncogene* 26(42):6238–6243.
58. Taichman RS, et al. (2002) Use of the stromal cell-derived factor-1/CXCR4 pathway in prostate cancer metastasis to bone. *Cancer Res* 62(6):1832–1837.
59. Knubel KH, et al. (2014) MerTK inhibition is a novel therapeutic approach for glioblastoma multiforme. *Oncotarget* 5(5):1338–1351.
60. Yakes FM, et al. (2011) Cabozantinib (XL184), a novel MET and VEGFR2 inhibitor, simultaneously suppresses metastasis, angiogenesis, and tumor growth. *Mol Cancer Ther* 10(12):2298–2308.
61. Ghilardi JR, et al. (2010) Administration of a tropomyosin receptor kinase inhibitor attenuates sarcoma-induced nerve sprouting, neuroma formation and bone cancer pain. *Mol Pain* 6:87.
62. Wilhelm SM, et al. (2008) Preclinical overview of sorafenib, a multikinase inhibitor that targets both Raf and VEGF and PDGF receptor tyrosine kinase signaling. *Mol Cancer Ther* 7(10):3129–3140.
63. Meyer A, et al. (2014) Role of sorafenib in overcoming resistance of chemotherapy-failure castration-resistant prostate cancer. *Clin Genitourin Cancer* 12(2):100–105.
64. Dahut WL, et al. (2008) A phase II clinical trial of sorafenib in androgen-independent prostate cancer. *Clin Cancer Res* 14(1):209–214.
65. Poulikakos PI, Zhang C, Bollag G, Shokat KM, Rosen N (2010) RAF inhibitors transactivate RAF dimers and ERK signalling in cells with wild-type BRAF. *Nature* 464(7287):427–430.
66. Zhao Y, Adjei AA (2014) The clinical development of MEK inhibitors. *Nat Rev Clin Oncol* 11(7):385–400.
67. Xin L, Ide H, Kim Y, Dubey P, Witte ON (2003) In vivo regeneration of murine prostate from dissociated cell populations of postnatal epithelia and urogenital sinus mesenchyme. *Proc Natl Acad Sci USA* 100(Suppl 1):11896–11903.
68. Loening AM, Gambhir SS (2003) AMIDE: A free software tool for multimodality medical image analysis. *Mol Imaging* 2(3):131–137.
69. Nguyen KQ, et al. (2014) Overexpression of MERTK receptor tyrosine kinase in epithelial cancer cells drives efferocytosis in a gain-of-function capacity. *J Biol Chem* 289(37):25737–25749.
70. Morrissey C, et al. (2013) Effects of androgen deprivation therapy and bisphosphonate treatment on bone in patients with metastatic castration-resistant prostate cancer: Results from the University of Washington Rapid Autopsy Series. *J Bone Miner Res* 28(2):333–340.

Supporting Information

Faltermeier et al. 10.1073/pnas.1521674112

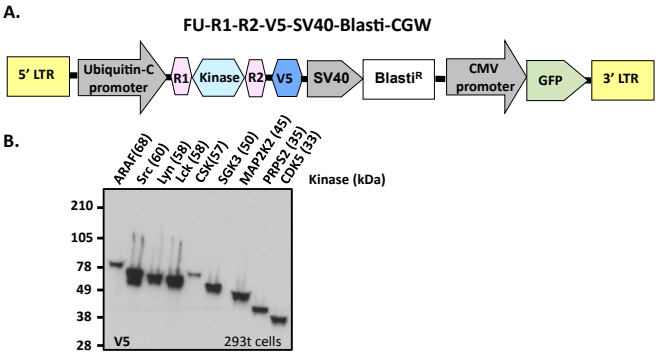

Fig. S1. Lentivirus-mediated overexpression of V5-tagged kinases. (*A*) Full-length kinases were cloned into the FU-R1-R2-V5-SV40-Blasti-CGW lentiviral vector shown. R1 and R2 represent recombination sites required for recombination-based Gateway cloning. LTR, Long-terminal repeat. (*B*) Western blot showing expression of selected kinases in 293t cells detected by a V5 antibody. The molecular mass of each kinase is indicated in parentheses.

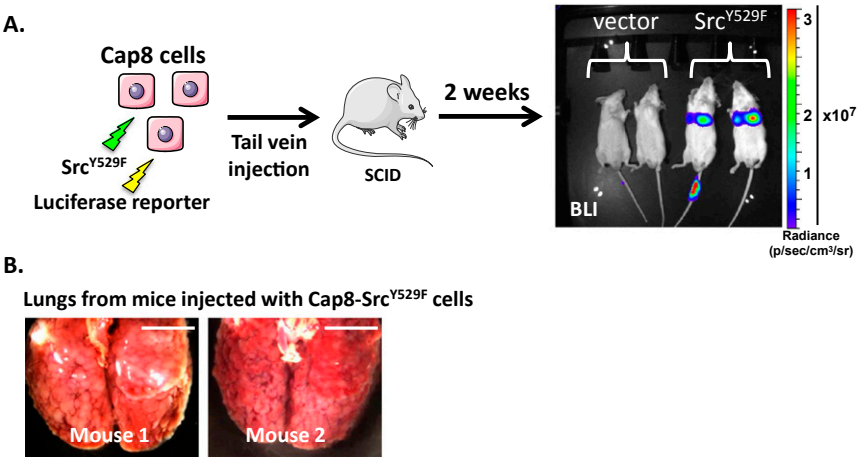

Fig. S2. Src^{Y529F} promotes lung colonization when overexpressed in murine prostate cells. (*A*) Experimental design to demonstrate that expression of mutationally activated kinase Src^{Y529F} in Cap8 cells promotes lung colonization. (*B*) Bright-field images of lungs removed from mice 3 wk after being injected with Cap8-Src^{Y529F} cells. (Scale bars, 5 mm.)

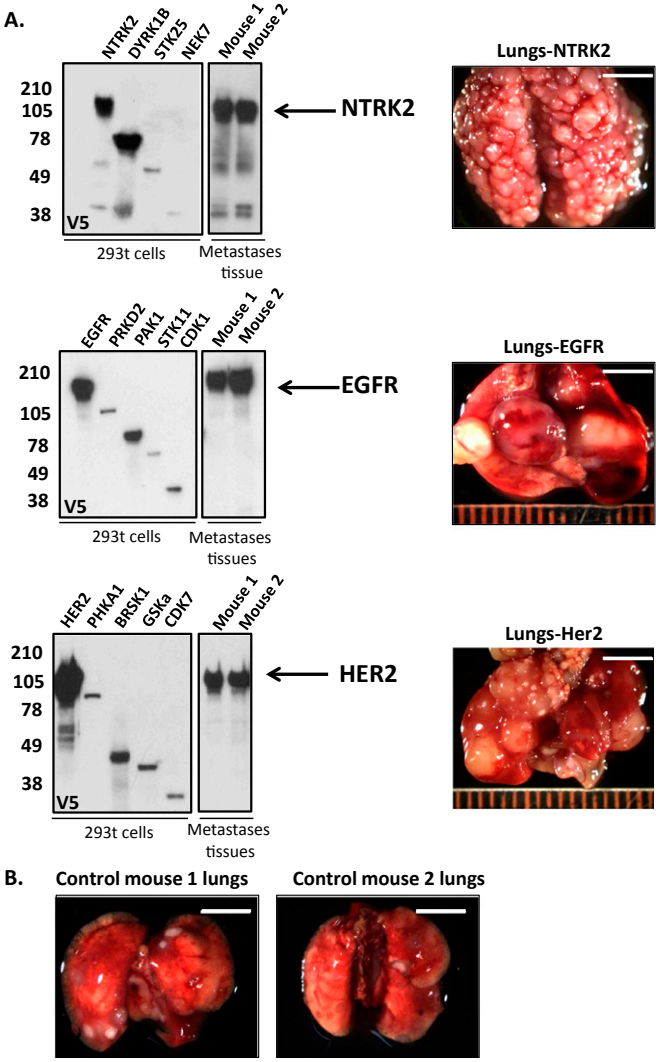

Fig. S3. Identification of kinases promoting lung colonization when expressed in murine prostate cells. (*A*, *Left*) Western blot analysis of lung tissues showing the specific kinase that was found to be enriched in lung metastasis. (*A*, *Right*) Representative bright-field images of tumor nodules in lungs from the corresponding mice. (Scale bars, 5 mm.) (*B*) Bright-field images of lungs removed from mice 10 wk after injection with control Cap8 cells. (Scale bars, 5 mm.)

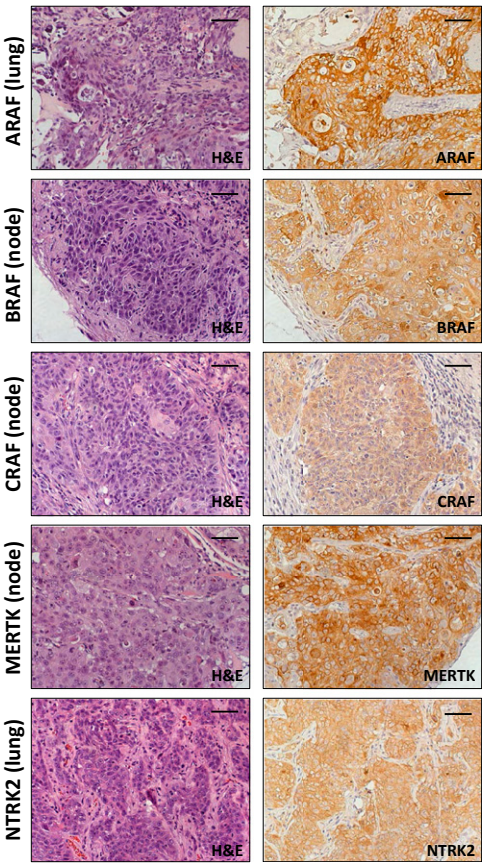

Fig. S4. Overexpression of kinases in RWPE-1 cells drives the formation of bone and visceral metastases. Representative histology of visceral (lung or lymph node) metastases removed from mice injected with RWPE-1 cells expressing RAF family members, MERTK, or NTRK2. (*Left*) H&E images. (*Right*) Corresponding kinase-specific staining. (Scale bars, 40 μm.) The histology of bone metastases removed from the same mice is shown in Fig. 4.

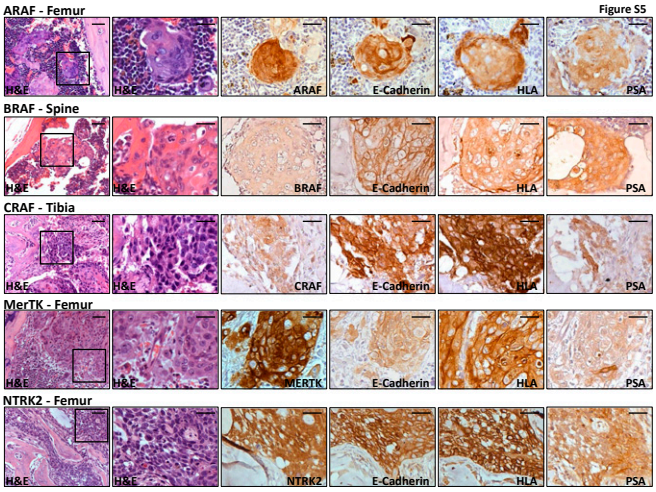

Fig. S5. Histological analysis of bones recovered from mice injected with cells expressing ARAF, BRAF, CRAF, MERTK, and NTRK2 confirms that metastases are of human prostate epithelial cell origin. (*Left* two columns) H&E stains of the affected bones removed from mice injected with RWPE-1 cells expressing the five metastasis-promoting kinases. Images in *Right* five columns are 20× magnification of the area outlined by a black box in the first column. (*Right* four columns) IHC staining of bone metastasis for overexpressed kinase, E-cadherin, HLA class I, and PSA. [Scale bars, 40 μm (*Left*) and 20 μm (*Right* five columns).]

Table S1. List and sources of the 125 kinases used in the screen

Kinase	pS, T, Y	cBioPortal	Literature
ABL	X		
ACVR2B		X	
ACVRL1		X	
ALK	X		
ARAF	X		
AXL	X		
BLK			X
BMP2K		X	
BMPR1A		X	
BMPR1B		X	
BMX	X		
BRAF	X		
BRSK1		X	
BTK		X	
CAMK2B		X	
CARD11		X	
CDC2 (CDK1)	X		
CDK10		X	
CDK2	X		
CDK3	X		
CDK4		X	
CDK5	X		
CDK6	X		
CDK9			X
CKB	X		
CSFR1	X		
Csk	X		
CSNK2A1	X		
DAPK1	X		
DDR1	X		
DGKB		X	
DYRK1b		X	
DYRK3		X	
EGFR	X		
EphA2		X	
EphA3	X		
EphA4	X		
EpHA6	X		
ERBB2	X		
ERBB3	X		
FASTK		X	
Fer			X
Fes	X		
FGFR1	X		
FGFR2			X
FGFR3			X
FLT1		X	
FLT3	X		
FLT4		X	
Fyn	X		
Gsk3A	X		
Hck	X		
INSRR			X
JAK1		X	
JAK3		X	
Lck	X		
LMTK2		X	
LYN	X		
MAP2K2	X		
MAP2K6		X	
MAP2K7	X		
MAP3K15		X	
MAP3K2	X		

Table S1. Cont.

Kinase	pS, T, Y	cBioPortal	Literature
MAP3K5	X		
MAP3K8			X
MAP4K3		X	
MAP4K4		X	
MAPK1	X		
MAPK12	X		
MAPK13	X		
MAPK14	X		
MAPK3	X		
MAPK8 (JNK1)	X		
MARK3		X	
MAST1		X	
MERTK			X
MET			X
MPP6		X	
MST1R		X	
Myt1	X		
NEK11		X	
NEK2		X	
NEK7		X	
NTRK2			X
NTRK3		X	
PAK1			X
PAK7			X
PCTK1		X	
PDGFRa	X		
PDGFRb	X		
PDK1	X		
PDK3			X
PHKA1		X	
PHKA2		X	
PIK3Ca		X	
PIK3CB		X	
PIM1			X
PRKD1			X
PRKD2			X
PRKX		X	
PRPF4B	X		
PRPS2		X	
PTK2		X	
PTK6	X		
RAF1	X		
RIPK2		X	
SGK2			X
SGK3		X	
SNX16		X	
Src	X		
SRPK1		X	
SRPK2		X	
SRPK3		X	
STK11			X
STK17B		X	
STK25		X	
STK3		X	
Syk	X		
TLK2		X	
TXK		X	
TYK2	X		
TYRO3		X	
ULK3			X
XYLB	X		

Listed are the 125 kinases evaluated in the in vivo screen, as well as the source from which they were identified: pS (serine), pY (tyrosine), pT (threonine): phosphoproteomics dataset; cBioPortal: genomic/RNA dataset; literature: PubMed.